Military Technical College
Kobry El-Kobba
Cairo, Egypt

12-th International Conference
on
Aerospace Sciences &
Aviation Technology

SHIELDING CHARACTERISTICS OF A PERIODIC CONDUCTING PATCH-ARRAY EMBEDDED IN AN INFINITE MULTILAYERED DIELECTRIC CYLINDRICAL STRUCTURE

Elregaily * H. A., Mohktar * M. M. and Allam * A. M.

ABSTRACT

A plane wave excitation of a periodic conducting patch-array embedded in an infinite multilayered dielectric cylinder, as a shielding structure, has been studied. Based on the Green's functions, the integral equation is formulated for describing the current on a conducting patch-array. Using Galerkin's method, the surface currents on the conducting patches are expanded in the form of series weighted Chebyshev polynomials of the first kind and the unknown coefficients are obtained by solving a resultant system of linear equations.
The validity of the formulation and the accuracy of the numerical solution are demonstrated for different array geometries. The numerical results depict the penetrated field, the scattered field and the shielding effectiveness for four different array geometries. Some of these results are compared to the simulated results using Zeland Fidelity Workshop (ZFW), and a good agreement was achieved.

Key word **–** Multilayered shielding, Galarkin's method, penetrated field, scattered field, shielding effectiveness.

***** Egyptian Armed Forces

I. Introduction

Coupling of electromagnetic energy into electronic devices and systems can cause electrical overstress to their internal circuits. This leads to failure, permanent degradation, or temporary malfunction (upset) of electronic devices and systems. Electromagnetic shielding is a technique that reduces the coupling of undesired radiated electromagnetic energy into equipment, so as to enable it to operate compatibly with its electromagnetic environment.

The reduction of coupling can be affected by shielding sensitive components and subsystems with a metallic enclosure, wherever practical. Obviously, the entire system cannot be shielded since antennas will not perform their intended functions when completely enclosed within a metallic shield. Another shielding mean to reduce coupling in a specified frequency band without affecting the characteristics of the antennas includes the shielding by using structures consisting of apertures / patches that acts as a filter to electromagnetic energy at frequencies outside the frequency band of interest for the system.

Three methods for determining the field which penetrates conducting cylinders containing narrow axially conducting slots for both TE- and TM- polarizations have been introduced by Chalmers and Butler [1, 2]. Firstly, is the scatterer method that treats the body as a scatterer and determines the interior field as the sum of the incident field produced by known source and the scattered field produced by the current in the body. Secondly, the short – circuit current method is based upon the field equivalence theorem, which allows one to change the excitation of the structure from the known source or incident field to an equivalent surface current placed on the aperture. The penetrated field can be determined by a procedure similar to that of scatterer method. Thirdly, the equivalent current method employs the equivalence principle to solve the equivalent magnetic currents and determine the field by knowledge of these currents. In all these methods integral equations are derived, that when solved by using method of moments yield currents from which penetrated field can be determined.

On the other hand, another cylindrical structure, consisting of multiple aperture system has been studied by Wen-Yan Yin et al [3]. They investigate the TEz-polarized plane wave penetrating through multilayered cylindrical cavity-backed apertures. The mathematical procedure is based on the direct integral equation technique combined with Galerkin's procedure, that can be solved numerically for the magnetic currents on the surround multiple apertures. More recently, they use the same technique to describe the near – zone field characteristics of TMz plane wave penetrating through cylindrical multiple apertures coated or covered with lossy or lossless media [4].

In our previous work [5], the shielding performance of an infinitely extended conducting strip-array embedded in multilayer dielectric cylindrical structure and excited by TMz – polarized plane wave has been considered. Based on the Green's functions, the integral equation is derived for describing the electric current distribution on the conducting strips. By using the Galerkin's procedure and taken into

consideration the edge effect of the conducting strips, the surface currents are expanded in the form of series weighted Chebyshev polynomials of the first kind.

This work is devoted to the problem of TMz – polarized plane wave excitation of a periodic conducting patch-array embedded in an infinite multilayer dielectric cylindrical structure. By using the same technique as in [5], the penetrated field, scattered field and shielding effectiveness is studied for different array geometries. Some of the results are compared to the simulated results using Zeland Fidelity Workshop (ZFW). This paper is organized as follow. Section II includes the formulation of the problem to obtain the integral equations for describing the electric current distributions on the conducting patches. Section III presents the numerical solution for these integral equations. The numerical results are analyzed in section IV. Finally, section V summarizes the paper.

II. Formulation

Figure 1 shows a periodic conducting patch-array embedded in multilayer dielectric cylindrical structure at, $\rho = R'_3$ ($R_2 \le R'_3 \le R_3$). The location of each patch is defined in the ϕ-direction by [$\psi_{2S\phi-1}$, $\psi_{2S\phi}$] and in the z-direction by [L_{2Sz-1} , L_{2Sz}] where s_ϕ, s_z are the patch numbers in ϕ- and z-directions respectively (s_ϕ = 1, 2…, s_z = 1, 2…). The regions ($\rho < R_1$) and ($\rho > R_3$) are usually a free space with parameters ε_o and μ_o.

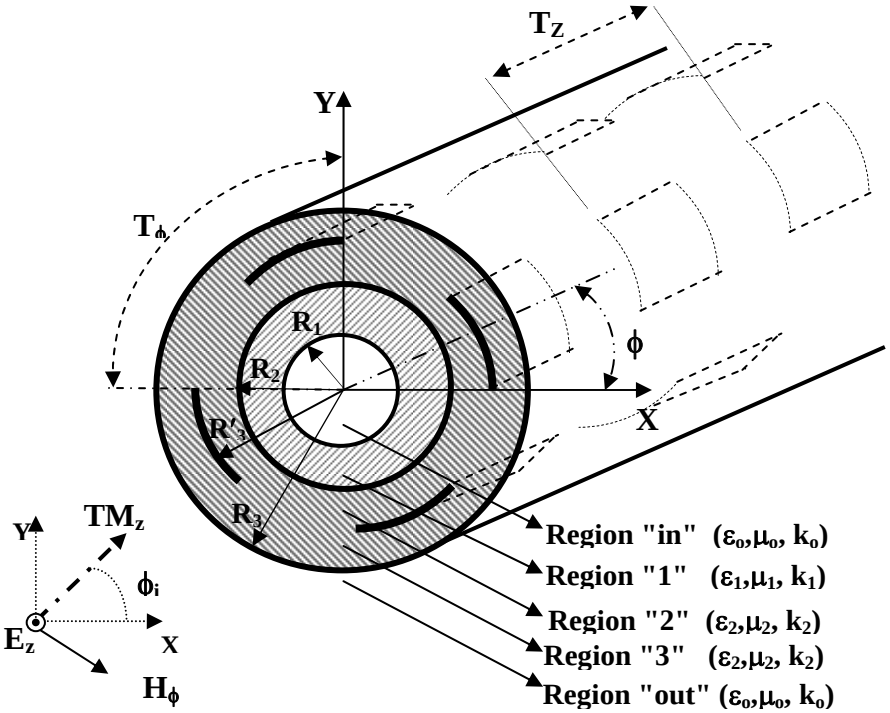

Fig. 1 Multilayered infinite dielectric cylinder with periodic conducting patches - array embedded at ($\rho = R'_3$).

For TMz–polarization, the normally incident electric and magnetic field components [4] is expressed as:

$$E_z^{(inc)} = E_o \sum_{m=-\infty}^{\infty} j^{-m} J_m(K_o\rho) e^{jm(\phi-\phi_{in})} \qquad (1\text{-a})$$

$$H_\phi^{(inc)} = -\frac{jE_o}{\eta_o} \sum_{m=-\infty}^{\infty} j^{-m} J'_m(K_o\rho) e^{jm(\phi-\phi_{in})} \qquad (1\text{-b})$$

where, $K_\circ = \omega\sqrt{\mu_\circ\varepsilon_\circ}$, $\eta_\circ = \sqrt{\mu_\circ/\varepsilon_\circ}$, ϕ_{in} is the angle of incidence measured from the x-axis, $J_m(K_\circ\rho)$ is the cylindrical Bessel function of the first kind m^{th} order and the prim denotes the derivative with respect to the argument ($K\rho$).

A. Excitation field expansion:

In the absence of the conducting patch array, the excitation field in each region can be described as:

$$E_z^{(i)} = E_o \sum_{m=-\infty}^{\infty} j^{-m} [\tilde{A}_m^{(i)} H_m^{(2)}(K_i\rho) + \tilde{B}_m^{(i)} J_m(K_i\rho)] e^{jm(\phi-\phi_{in})} \qquad (2\text{-a})$$

$$H_\phi^{(i)} = -\frac{jE_o}{\eta_o} \sum_{m=-\infty}^{\infty} j^{-m} [\tilde{A}_m^{(i)} H_m^{(2)'}(K_i\rho) + \tilde{B}_m^{(i)} J'_m(K_i\rho)] e^{jm(\phi-\phi_{in})} \qquad (2\text{-b})$$

where, $\tilde{A}_m^{(in)} = \tilde{B}_m^{(out)} = 0$, $K_i = \omega\sqrt{\mu_i\varepsilon_i}$ and $H_m^{(2)}(K_i\rho)$ is Hankel function of second kind and order m,

$$i = \begin{cases} in & (\rho \le R_1) \\ tr_1 & (R_1 \le \rho \le R_2) \\ tr_2 & (R_2 \le \rho \le R_3) \\ out & (\rho \ge R_3) \end{cases}$$

and the unknown coefficients $\tilde{A}_m^{(out)}, \tilde{A}_m^{(tr_1)}, \tilde{B}_m^{(tr_1)}, \tilde{A}_m^{(tr_2)}, \tilde{B}_m^{(tr_2)}$ and $\tilde{B}_m^{(in)}$ are all determined by applying the boundary conditions for tangential components of the electric and magnetic fields at $\rho = R_1$, R_2 and R_3 [5].

B. Green's functions formulation:

Let we have a curved rectangular patches embedded at $\rho = R_3^{'}$ that are uniformly periodic with periodicity T_ϕ and T_z in ϕ- and z-directions respectively, as shown in Fig.1. The Z–components of the scattered electric and magnetic fields in each region due to the induced surface currents J_z and J_ϕ on the conductor surface can be expressed as [6],

$$E_{zs}^{(\nu)}(\rho,\phi,z)=\sum_{m=-\infty}^{\infty}\sum_{n=-\infty}^{\infty}[\tilde{A}_{\nu mn}J_m(K_{\nu\rho_n}\rho)+\tilde{B}_{\nu mn}H_m^{(2)}(K_{\nu\rho_n}\rho)]e^{jm\phi}e^{jK_{zn}Z} \quad (3\text{-a})$$

$$H_{zs}^{(\nu)}(\rho,\phi,z)=\sum_{m=-\infty}^{\infty}\sum_{n=-\infty}^{\infty}[\tilde{C}_{\nu mn}J_m(K_{\nu\rho_n}\rho)+\tilde{D}_{\nu mn}H_m^{(2)}(K_{\nu\rho_n}\rho)]e^{jm\phi}e^{jK_{zn}Z} \quad (3\text{-b})$$

$$\text{where, } \nu=\begin{cases}\text{in} & (\rho\le R_1)\\ 1 & (R_1\le\rho\le R_2)\\ 2 & (R_2\le\rho\le R_3')\\ 3 & (R_3'\le\rho\le R_3)\\ \text{out} & (\rho\ge R_3)\end{cases},$$

$\tilde{B}_{in_{mn}}=\tilde{D}_{in_{mn}}=\tilde{A}_{out_{mn}}=\tilde{C}_{out_{mn}}=0$, $K_{zn}=2\pi n/T_z$, $K_\nu^2=K_{\nu\rho_n}^2+K_{zn}^2$ and $K_\nu=\omega\sqrt{\mu_\nu\varepsilon_\nu}$

Once E_z and H_z are known, the scattered field components of E_ρ , E_ϕ , H_ρ and H_ϕ in each region can be obtained through the following expressions [6],

$$E_\rho=\frac{j[K_z(\partial E_z/\partial\rho)+(\omega\mu_o/\rho)(\partial H_z/\partial\phi)]}{K_{\nu\rho}^2} \qquad E_\phi=\frac{j[(K_z/\rho)(\partial E_z/\partial\phi)-\omega\mu_o(\partial H_z/\partial\rho)]}{K_{\nu\rho}^2}$$

$$H_\rho=\frac{j[(-\omega\varepsilon_i/\rho)(\partial E_z/\partial\phi)+K_z(\partial H_z/\partial\rho)]}{K_{\nu\rho}^2} \qquad H_\phi=\frac{j[\omega\varepsilon_i(\partial E_z/\partial\rho)+(K_z/\rho)(\partial H_z/\partial\phi)]}{K_{\nu\rho}^2}$$

The continuity of the electric and magnetic fields on the inner and outer surfaces of the structure requires that:

at ($\rho = R_1$);

$$E_{zs}^{(1)}=E_{zs}^{(in)},\ H_{zs}^{(1)}=H_{zs}^{(in)}$$
$$E_{\phi s}^{(1)}=E_{\phi s}^{(in)},\ H_{\phi s}^{(1)}=H_{\phi s}^{(in)}$$

at ($\rho = R_2$);

$$E_{zs}^{(2)}=E_{zs}^{(1)},\ H_{zs}^{(2)}=H_{zs}^{(1)}$$
$$E_{\phi s}^{(2)}=E_{\phi s}^{(1)},\ H_{\phi s}^{(2)}=H_{\phi s}^{(1)}$$

at ($\rho = R'_3$) ;

$$E_{zs}^{(3)}=E_{zs}^{(2)},\ H_{zs}^{(3)}-H_{zs}^{(2)}=J_\phi$$
$$E_{\phi s}^{(3)}=E_{\phi s}^{(2)},\ H_{\phi s}^{(3)}-H_{\phi s}^{(2)}=J_z$$

at ($\rho = R_3$);

$$E_{zs}^{(out)}=E_{zs}^{(3)},\ H_{zs}^{(out)}=H_{zs}^{(3)}$$
$$E_{\phi s}^{(out)}=E_{\phi s}^{(3)},\ H_{\phi s}^{(out)}=H_{\phi s}^{(3)}$$

Applying the above boundary conditions, the unknown coefficients $\tilde{A}_{\nu mn}$, $\tilde{B}_{\nu mn}$, $\tilde{C}_{\nu mn}$ and $\tilde{D}_{\nu mn}$ (16 - unknowns) can be determined in terms of the unknown current densities $\tilde{J}_{z_{mn}}$ and $\tilde{J}_{\phi_{mn}}$. Substituting by these coefficients in Eqn.(3), the scattered fields in the five regions can be expressed as,

$$E_{zs}^{(\nu)}(\rho,\phi,z)=\sum_{m=-\infty}^{\infty}\sum_{n=-\infty}^{\infty}\left(G_{z\phi_{mn}}^{(\nu)}\tilde{J}_{\phi_{mn}}+G_{zz_{mn}}^{(\nu)}\tilde{J}_{z_{mn}}\right)e^{jm\phi}e^{jK_{zn}Z} \quad (4\text{-a})$$

$$E_{\phi s}^{(\nu)}(\rho,\phi,z)=\sum_{m=-\infty}^{\infty}\sum_{n=-\infty}^{\infty}\left(G_{\phi\phi_{mn}}^{(\nu)}\tilde{J}_{\phi_{mn}}+G_{\phi z_{mn}}^{(\nu)}\tilde{J}_{z_{mn}}\right)e^{jm\phi}e^{jK_{zn}Z} \quad (4\text{-b})$$

where,

$$\tilde{J}_{\phi_{mn}}=\frac{1}{T_\phi T_z}\int_0^{T_\phi}\int_0^{T_z}J_\phi e^{-jm\phi}e^{-jK_{zn}Z}dK_{zn}d\phi \quad (5\text{-a})$$

$$\tilde{J}_{z_{mn}}=\frac{1}{T_\phi T_z}\int_0^{T_\phi}\int_0^{T_z}J_z e^{-jm\phi}e^{-jK_{zn}Z}dK_{zn}d\phi \quad (5\text{-b})$$

is the mn$^{\underline{th}}$. coefficient of the Fourier expansion of the induced current on the conducting patches in $\hat{\phi}$ and $\hat{z}$ respectively, $G_{z\phi_{mn}}^{(\nu)}$, $G_{zz_{mn}}^{(\nu)}$, $G_{\phi\phi_{mn}}^{(\nu)}$, and $G_{\phi z_{mn}}^{(\nu)}$ are the Green's functions for different regions, which can be calculated by applying the same procedures used in [5] for the two-dimensional Green's functions, and T_ϕ and T_z are the patches periodicities in $\hat{\phi}$ and $\hat{z}$ respectively [$T_\phi=2\pi/P_\phi$, $T_z=R'_3\times T_\phi/2$].

C. Boundary conditions:

Boundary conditions on the surface of the conductor at $\rho=R_3^{'}$ can be written as,

$$E_z^{(tr2)}(R_3^{'})=-E_{zs}^{(2)}(R_3^{'})=-\sum_{m=-\infty}^{\infty}\sum_{n=-\infty}^{\infty}\left(G_{z\phi_{mn}}^{(2)}\tilde{J}_{\phi_{mn}}+G_{zz_{mn}}^{(2)}\tilde{J}_{z_{mn}}\right)e^{jm\phi}e^{jK_{zn}Z} \quad (6\text{-a})$$

$$0\quad=E_{\phi s}^{(2)}(R_3^{'})=\sum_{m=-\infty}^{\infty}\sum_{n=-\infty}^{\infty}\left(G_{\phi\phi_{mn}}^{(2)}\tilde{J}_{\phi_{mn}}+G_{\phi z_{mn}}^{(2)}\tilde{J}_{z_{mn}}\right)e^{jm\phi}e^{jK_{zn}Z} \quad (6\text{-b})$$

To solve the integral equations of (6). Galerkin's moment method is applied. To begin with, we first expand the unknown surface current densities on the conducting patches J_z and J_ϕ in terms of linear combinations of known basis functions as:

$$J_\phi=\sum_{s_z=1}^{P_z}\sum_{s_\phi=1}^{P_\phi}\sum_{q_{z_1}=0}^{Q_{z_1}}\sum_{q_{\phi_1}=0}^{Q_{\phi_1}}a_{q(z,\phi)}^{s(z,\phi)}\frac{T_{q_{z_1}}(y_{os_z}^{'})}{\sqrt{1-y_{os_z}^{'2}}}\mathrm{Sin}(q_{\phi_1}\frac{\pi}{2}x_{os_\phi}^{''}) \quad (7\text{-a})$$

$$J_z=\sum_{s_z=1}^{P_z}\sum_{s_\phi=1}^{P_\phi}\sum_{q_{z_2}=0}^{Q_{z_2}}\sum_{q_{\phi_2}=0}^{Q_{\phi_2}}b_{q(z,\phi)}^{s(z,\phi)}\frac{T_{q_{\phi_2}}(x_{os_\phi}^{'})}{\sqrt{1-x_{os_\phi}^{'2}}}\mathrm{Sin}(q_{z_2}\frac{\pi}{2}y_{os_z}^{''}) \quad (7\text{-b})$$

where, $T_{q_{z_1}}(y_{os_z}^{'})$ and $T_{q_{\phi_2}}(x_{os_\phi}^{'})$..... are Chebyshev polynomials of the first kind,

$1/\sqrt{1-y'^{2}_{os_z}}$ and $1/\sqrt{1-x'^{2}_{os_\phi}}$ ....are the factors represent the edge effect for each patch in the z- and ϕ- directions respectively,

$$x'_{os_\phi}=\frac{\phi'-(\psi_{2s_\phi}+\psi_{2s_\phi-1})/2}{(\psi_{2s_\phi}-\psi_{2s_\phi-1})/2}\ ,\qquad y'_{os_z}=\frac{z'-(L_{2s_z}+L_{2s_z-1})/2}{(L_{2s_z}-L_{2s_z-1})/2}$$

$$x''_{os_\phi}=x'_{os_\phi}+1\ ,\qquad y''_{os_z}=y'_{os_z}+1$$

and $a^{s(z,\phi)}_{q(z,\phi)}$ and $b^{s(z,\phi)}_{q(z,\phi)}$ ...are the unknown expanding coefficients to be determined.

Substituting by Eqns. (5-a) and (7-a) into Eqn. (6-a) gives,

$$E_z^{(tr2)}(R'_3)=\frac{1}{T_\phi T_z}\sum_{m=-\infty}^{\infty}\sum_{n=-\infty}^{\infty}e^{jm\phi}e^{jK_{zn}Z}$$

$$\left(G^{(2)}_{z\phi mn}\sum_{s_z=1}^{P_z}\sum_{s_\phi=1}^{P_\phi}\sum_{q_{z1}=0}^{Q_{z1}}\sum_{q_{\phi1}=0}^{Q_{\phi1}}a^{s(z,\phi)}_{q(z,\phi)}\int_0^{T_\phi}\int_0^{T_z}\frac{T_{q_{z1}}(y'_{os_z})}{\sqrt{1-y'^{2}_{os_z}}}\mathrm{Sin}(q_{\phi_1}\frac{\pi}{2}x''_{os_\phi})e^{-jm\phi}e^{-jK_{zn}Z}dK_{zn}d\phi\right)$$

$$\left(G^{(2)}_{zzmn}\sum_{s_z=1}^{P_z}\sum_{s_\phi=1}^{P_\phi}\sum_{q_{z2}=0}^{Q_{z2}}\sum_{q_{\phi2}=0}^{Q_{\phi2}}b^{s(z,\phi)}_{q(z,\phi)}\int_0^{T_\phi}\int_0^{T_z}\frac{T_{q_{\phi2}}(x'_{os_\phi})}{\sqrt{1-x'^{2}_{os_\phi}}}\mathrm{Sin}(q_{z_2}\frac{\pi}{2}y''_{os_z})e^{-jm\phi}e^{-jK_{zn}Z}dK_{zn}d\phi\right)$$

(8-a)

Substituting by Eqns. (5-b) and (7-b) into Eqn. (6-b) gives,

$$0=\frac{1}{T_\phi T_z}\sum_{m=-\infty}^{\infty}\sum_{n=-\infty}^{\infty}e^{jm\phi}e^{jK_{zn}Z}$$

$$\left(G^{(2)}_{\phi\phi mn}\sum_{s_z=1}^{P_z}\sum_{s_\phi=1}^{P_\phi}\sum_{q_{z1}=0}^{Q_{z1}}\sum_{q_{\phi1}=0}^{Q_{\phi1}}a^{s(z,\phi)}_{q(z,\phi)}\int_0^{T_\phi}\int_0^{T_z}\frac{T_{q_{z1}}(y'_{os_z})}{\sqrt{1-y'^{2}_{os_z}}}\mathrm{Sin}(q_{\phi_1}\frac{\pi}{2}x''_{os_\phi})e^{-jm\phi}e^{-jK_{zn}Z}dK_{zn}d\phi\right)$$

$$\left(G^{(2)}_{\phi zmn}\sum_{s_z=1}^{P_z}\sum_{s_\phi=1}^{P_\phi}\sum_{q_{z2}=0}^{Q_{z2}}\sum_{q_{\phi2}=0}^{Q_{\phi2}}b^{s(z,\phi)}_{q(z,\phi)}\int_0^{T_\phi}\int_0^{T_z}\frac{T_{q_{\phi2}}(x'_{os_\phi})}{\sqrt{1-x'^{2}_{os_\phi}}}\mathrm{Sin}(q_{z_2}\frac{\pi}{2}y''_{os_z})e^{-jm\phi}e^{-jK_{zn}Z}dK_{zn}d\phi\right)$$

(8-b)

III. Numerical solution:

By adopting Galerkin's procedures, both sides of Eqn. (8-a) are multiplied by the factor $\frac{T_{\nu 1}(y_{os_{z1}})}{\sqrt{1-y_{os_{z1}}^2}}\mathrm{Sin}(q_{\nu 11}\pi x_{os_{\phi 1}})$, ν_1 =0,1,2, ...Q_{z1} , ν_{11} =0,1,2, …..$Q_{\phi 1}$ for each patch at $y_{os_{z1}} = \frac{z-(L_{2s_z}+L_{2s_z-1})/2}{(L_{2s_z}-L_{2s_z-1})/2}$, $x_{os_{\phi 1}} = \frac{\phi-(\psi_{2s_\phi}+\psi_{2s_\phi-1})/2}{(\psi_{2s_\phi}-\psi_{2s_\phi-1})/2}+1$, and integrating over regions $\phi \in [\psi_{2s_\phi-1}, \psi_{2s_\phi}]$ and $Z \in [L_{2s_z-1}, L_{2s_z}]$ respectively. Then,

$$E_o \sum_{m=-\infty}^{\infty} \sum_{s_z=1}^{P_z} \sum_{s_\phi=1}^{P_\phi} \sum_{\nu_1=0}^{Q_{z_1}} \sum_{\nu_{11}=0}^{Q_{\phi_1}}$$

$$\left(j^{-m}[\tilde{A}_m^{(2)} H_m^{(2)}(K_2 R_3^{'}) + \tilde{B}_m^{(2)} J_m(K_2 R_3^{'})] \int_0^{T_z}\int_0^{T_\phi} \frac{T_{\nu 1}(y_{os_z})}{\sqrt{1-y_{os_z}^2}} \mathrm{Sin}(q_{\nu 11}\pi x_{os_\phi}) e^{jm(\phi-\phi_{in})} dK_{zn} d\phi \right)$$

$$= \sum_{m=-\infty}^{\infty} \sum_{n=-\infty}^{\infty} (J_{zspt}) \left(G_{z\phi_{mn}}^{(2)} a_{q(z,\phi)}^{s(z,\phi)} (J_{\phi spc}) + G_{zz_{mn}}^{(2)} b_{q(z,\phi)}^{s(z,\phi)} (J_{zspc}) \right) \qquad (9\text{-a})$$

Similarly, by multiplying both sides of Eqn. (11-b) by the factor, $\frac{T_{\nu 2}(x_{os_{\phi 2}})}{\sqrt{1-x_{os_{z2}}^2}}\mathrm{Sin}(q_{\nu 22}\pi y_{os_{z2}})$, ν_2 =0,1,2,.... $Q_{\phi 2}$, ν_{22} =0,1,2, …Q_{z2} for each patch at $y_{os_{z2}} = \frac{z-(L_{2s_z}+L_{2s_z-1})/2}{(L_{2s_z}-L_{2s_z-1})/2}+1$, $x_{os_{\phi 2}} = \frac{\phi-(\psi_{2s_\phi}+\psi_{2s_\phi-1})/2}{(\psi_{2s_\phi}-\psi_{2s_\phi-1})/2}$ and integrating over regions $\phi \in [\psi_{2s_\phi-1}, \psi_{2s_\phi}]$ and $Z \in [L_{2s_z-1}, L_{2s_z}]$ respectively. Then,

$$0 = \sum_{m=-\infty}^{\infty} \sum_{n=-\infty}^{\infty} (J_{\phi spt}) \left(G_{\phi\phi_{mn}}^{(2)} a_{q(z,\phi)}^{s(z,\phi)} (J_{\phi spc}) + G_{\phi z_{mn}}^{(2)} b_{q(z,\phi)}^{s(z,\phi)} (J_{zspc}) \right) \qquad (9\text{-b})$$

where,

$$J_{\phi spc} = \frac{1}{T_z T_\phi} \sum_{s_z=1}^{P_z} \sum_{s_\phi=1}^{P_\phi} \sum_{\nu_1=0}^{Q_{z1}} \sum_{\nu_{11}=0}^{Q_{\phi_1}} \int_0^{T_\phi}\int_0^{T_z} \frac{T_{\nu 1}(y_{os_{z1}})}{\sqrt{1-y_{os_{z1}}^2}} \mathrm{Sin}(\nu_{11}\pi x_{os_{\phi 1}}) e^{jm\phi} e^{jK_{zn}Z} dK_{zn} d\phi \qquad (10\text{-a})$$

is the spectral amplitude of the current basis function in ϕ-direction.

$$J_{\phi spt} = \frac{1}{T_z T_\phi} \sum_{s_z=1}^{P_z} \sum_{s_\phi=1}^{P_\phi} \sum_{q_{z_1}=0}^{Q_{z1}} \sum_{q_{\phi 1}=0}^{Q_{\phi_1}} \int_0^{T_\phi}\int_0^{T_z} \frac{T_{q_{z1}}(y'_{os_z})}{\sqrt{1-y'^2_{os_z}}} \mathrm{Sin}(q_{\phi 1}\pi x'_{os_\phi}) e^{-jm\phi} e^{-jK_{zn}Z} dK_{zn} d\phi \qquad (10\text{-b})$$

is the spatial amplitude of the current basis function in ϕ-direction.

^

$$J_{zspc}=\frac{1}{T_zT_\phi}\sum_{s_z=1}^{P_z}\sum_{s_\phi=1}^{P_\phi}\sum_{\nu_{22}=0}^{Q_{z_2}}\sum_{\nu_{2=0}}^{Q_{\phi_2}}\int_0^{T_\phi}\int_0^{T_z}\frac{T_{\nu 2}(x_{os_{\phi 2}})}{\sqrt{1-x_{os_{\phi 2}}^2}}\mathrm{Sin}(\nu_{22}\pi y_{os_{z2}})e^{jm\phi}e^{jK_{zn}Z}dK_{zn}d\phi \qquad (10\text{-c})$$

is the spectral amplitude of the current basis function in Z-direction.

$$J_{zspt}=\frac{1}{T_zT_\phi}\sum_{s_z=1}^{P_z}\sum_{s_\phi=1}^{P_\phi}\sum_{q_{z_2}=0}^{Q_{z_2}}\sum_{q_{\phi 2}=0}^{Q_{\phi_2}}\int_0^{T_\phi}\int_0^{T_z}\frac{T_{q_{\phi 2}}(x'_{os_\phi})}{\sqrt{1-x'^2_{os_\phi}}}\mathrm{Sin}(q_{z_2}\pi y'_{os_z})e^{-jm\phi}e^{-jK_{zn}Z}dK_{zn}d\phi \qquad (10\text{-d})$$

is the spatial amplitude of the current basis function in Z-direction.
Equations (9-a) and (9-b) can be represented as a system of linear equations which can be written in matrix form as:

$$\begin{bmatrix}LHS_z\\0\end{bmatrix}=\begin{bmatrix}RHS_{z\phi} & RHS_{zz}\\RHS_{\phi\phi} & RHS_{\phi z}\end{bmatrix}\begin{bmatrix}a\\b\end{bmatrix}$$

Where,

[LHS] …is one column-array with dimension $1\times\ [P_z\times P_\phi\times(Q_{z1}\times Q_{\phi 1}+ Q_{z2}\times Q_{\phi 2})]$,

[RHS]…is a matrix with dimensions

$$[P_z\times P_\phi\times(Q_{z1}\times Q_{\phi 1}+ Q_{z2}\times Q_{\phi 2})]\times[P_z\times P_\phi\times(Q_{z1}\times Q_{\phi 1}+ Q_{z2}\times Q_{\phi 2})],\quad \text{and}$$

(a, b)… is the current amplitude coefficients which can be determined as:

$$\begin{bmatrix}a\\b\end{bmatrix}=\begin{bmatrix}RHS_{z\phi} & RHS_{zz}\\RHS_{\phi\phi} & RHS_{\phi z}\end{bmatrix}^{-1}\begin{bmatrix}LHS_z\\0\end{bmatrix} \qquad (11)$$

IV. Numerical results:

Based on the above mathematical treatment, computer codes have been developed for calculating the shielding characteristics of the structure in Fig.1. Let R_1=0.2m, R_2=0.25m, R'_3=0.27m and R_3=0.3m, while the constitutive parameters are ε_{r1}=1.5, ε_{r2}=2.5 and $\mu_{r1}=\mu_{r2}$=1. Consider the case of plane wave excitation with ϕ_{in}=90° and frequency f = 100 MHz. The array embedded at R'$_3$, have angular width (T_ϕ/2) and length (T_z/2) for the conductors.

The validity of the formulated and written codes including the accuracy of the numerical solution has been fulfilled by computing the current and field distributions on the surface containing the conducting patches. According to numerical experiments and convergence study, $Q_{z1}=Q_{\phi 2}$=30 and $Q_{z2}=Q_{\phi 1}$=10 are employed for expanding the currents, and the field modes are truncated to M=N=20, (m=-M:M, n=-N:N).

Figure 2 depicts a three dimensional patterns of the penetrated electric fields for the cases of one, two, three and four patch-arrays. It shows that the penetrated field satisfy the boundary conditions at the conductor surface and the penetration of the cross component $|E_\phi|$ is much smaller than that of the copolar one $|E_z|$. It also shows that $|E_z|$ gives a considerable high level of the penetrated fields near the center of the cylindrical structure for all cases. This gives a good estimation for a low shielding performance at such frequency (f=100 MHz).

The normalized amplitudes of the far zone scattered fields for the same cases are illustrated in Fig.3. The calculated results (the case of infinitely extended structure) are compared with the simulated one (structure with length 5λ) using Zeland Fidelity Workshop (ZFW) and a good agreement was found. The figure also shows the simulation result for complete conducting cylinder, embedded at R'_3, as an ideal shielding case. We can see that the results are far from the ideal case at 100MHz which agree with the penetrated field results that the structure at this frequency gives low shielding performance.

One of the very important parameters that are used to determine the shielding performance of any shielding structure is the shielding effectiveness (SE). The SE is defined as the ratio of the field strength in the presence and absence of the shielding structure. However, for cylindrical nature of the structure one has to expect a variation in the (SE) with the transversal angle (ϕ), longitudinal length (z) and radial distance (ρ). In this work the variation with ρ is presented for the case of normal incidence, at fixed position in z and ϕ. The variation of SE with the frequency is also studied. The SE is calculated for the electric field (SE_e), the magnetic field (SE_h) and the power density (SE_p).

Figures 4, 5 depict the SE_e, SE_h and SE_p for the four studied structures near the center (ρ=0.05 m) and at the boundary containing the conducting surface (ρ=0.27 m) respectively. For each location two cases are presented, the free-standing structure ($\varepsilon_{r1}=\varepsilon_{r2}=1$), the left hand side of the figures, and structure with supporting dielectric layers ($\varepsilon_{r1}=1.5$, $\varepsilon_{r2}=2.5$), the right hand side of the figures.

In Fig.4.a, the case of free-standing structure, a low shielding performance is obtained for the electric field (SE_e) in the frequency range below 300 MHz at the center with SE_h (-18 to -37dB) and SE_p (-9 to -19dB). At 677 MHz there is an obvious structure resonance at which one can notes narrow peaks in the three quantities that can be used for communication through the shielding structure. With increasing the number of patches, for the free-standing cases illustrated in Figs.4.b-d, where the length of the patch becomes shorter and the angular width becomes narrower, we can notice that the variation in the characteristic curves is reduced while the structure resonance (at 677 MHz) is shifted. It worth, noting that there is an increase in SE_e at some frequencies above 0dB that is mainly due multiple reflections inside the structure and the diffraction at edges. Also, the power shielding effectiveness (SE_p) at these frequencies does not exceed the 0 dB. In the presence of supporting layers with ($\varepsilon_{r1}=1.5$, $\varepsilon_{r2}=2.5$), the right hand side curves of Fig.4, the structure shows different shielding characteristics where the SE_e becomes more weak, the effect of multiple reflection and edges diffraction increases and the

variations in characteristic curves increases. Also, there is a lower shift in the resonance due to the effect of supporting dielectric layers of higher permittivity to be at 620 MHz for the case of one patch-array in Fig.4.a. This resonance is shifted up by increasing the number of patches as shown in Figs. 4.b-d

Near the surface of the conductor (at ρ=0.27 m), Fig.5.a illustrates the case of free-standing one patch-array. There is wide dip in the frequency range (450-850 MHz) compared to that near the center shown in Fig.4.a which is followed by surface resonance at 900 MHz. Increasing the number of patches has an effect on the width and position of this dip as illustrated in Figs.5.b-d. In the case of four patch-array, shown in Fig.5.d, a SE_p below -10 dB can be obtained at frequencies greater than 250 MHz and reaches -37 dB at 924 MHz. Figure 5 also depicts the SE curves near the conductor surface with the presence of supporting layers (ε_{r1}=1.5, ε_{r2}=2.5). We can see that the variations in characteristic curves increases due to the presence of the dielectric layers. Also, there are frequency regions that are convenient for shielding applications. In Fig.5.d, the four patch-array, there is a frequency region (220 MHz – 615 MHz) at which the power shielding (SE_p) is below -10 dB and reaches -35 dB at 392 MHz. The three patch-array, illustrated in Fig.5.c, the SE_p is below -10 dB in the frequency region (250 MHz - 550 MHz) and reaches -28 dB at 411 MHz. Also, in the case of two patch-array depicted in Fig.5.b, there is shallow dip at frequencies grater than 645MHz where the SE_p is less than -10 dB.

V. Conclusion:

In this paper, we have investigated the penetrated field, the scattered field and the shielding characteristics of a TMz plane wave excitation of one, two, three and four periodic conducting patch-arrays embedded in an infinite multilayer dielectric cylindrical structure. The applied technique, based on the Green's function combined with the Chebyshev polynomial with edge effect, is very efficient for such structures. Numerical results give a very good contribution which can be used for actual applications. It shows that the shielding operating bandwidth increases by increasing the number of conducting patches in the embedded array. It also shows that the shielding effectiveness near the surface containing the conductor is better than that at the center of the structure. A region in which SE_p is below -10 dB and reaches -35 dB in the frequency range from 220 MHz to 615 MHz is obtained near the conductor surface with the presence of supporting dielectric layers. Finally, the presence of dielectric layers causes shift to the resonance frequency and increase the multiple reflections inside the structure.

References:

[1] J. D. Shumpert and C. M. Butler, " Penetration through slots in conducting cylinders – Part1: TE case, " IEEE Trans. Antenna propagate., vol. AP-46, pp. 1612-1621, Nov. 1998.

[2] J. D.Shumpert and C. M. Butler, " Penetration through slots in conducting cylinders – Part2: TM case, " IEEE Trans. Antenna propagate., vol. AP-46, pp. 1622-1628, Nov. 1998.

[3] W. Yin, L. Li, T. You, and M. Leong, " Multiple penetration of a TEz – polarized plane wave into multilayered cylindrical cavity-backed apertures, "

IEEE Trans. Antenna propagate., vol. AP-42, pp. 330-338, Nov. 2000.

[4] W. Yin, L. Li, T. Yeo, M. Leong and P. Kooi, " The near-zone field characteristics of an E-polarization plane wave penetrating through cylindrical multiple apertures (non) coated with lossy and lossless media, " IEEE Trans. Antenna propagate., vol. AP-44, pp. 329-337, May. 2002.

[5] Elregaily H. A., Mohktar M. M. and Allam A. M., "Shielding characteristics of an infinitely extended conducting strip-array embedded in multilayered dielectric cylindrical structure," 5th ICEENG conf., Military Technical College-Egypt, AW-5, May 2006.

[6] Kin-Lu Wong, "Design of nonplaner microstrip antennas and transmission lines", John Wiley & Sons, Inc., 1999.

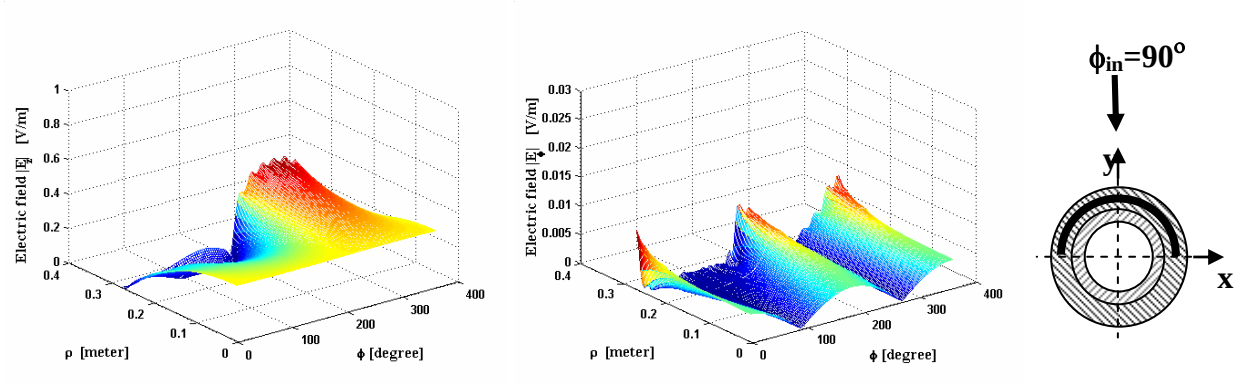

(a) One patch-array.

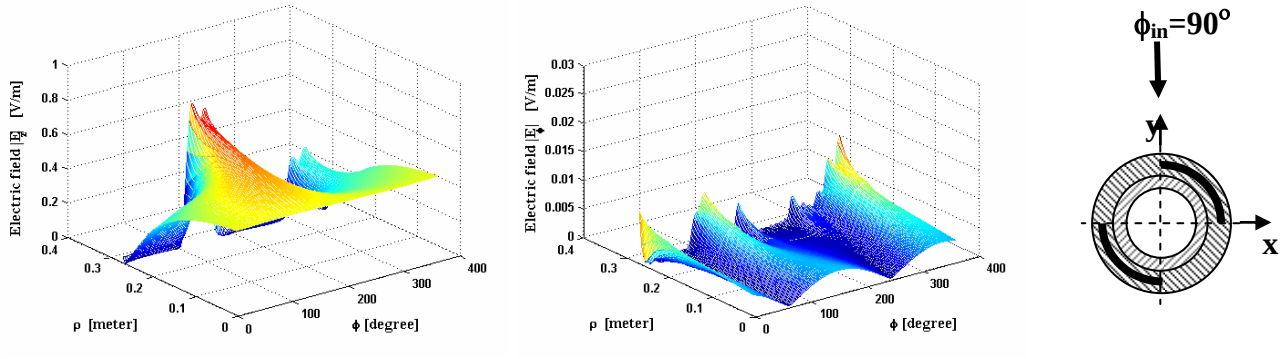

(b) Two patch-array.

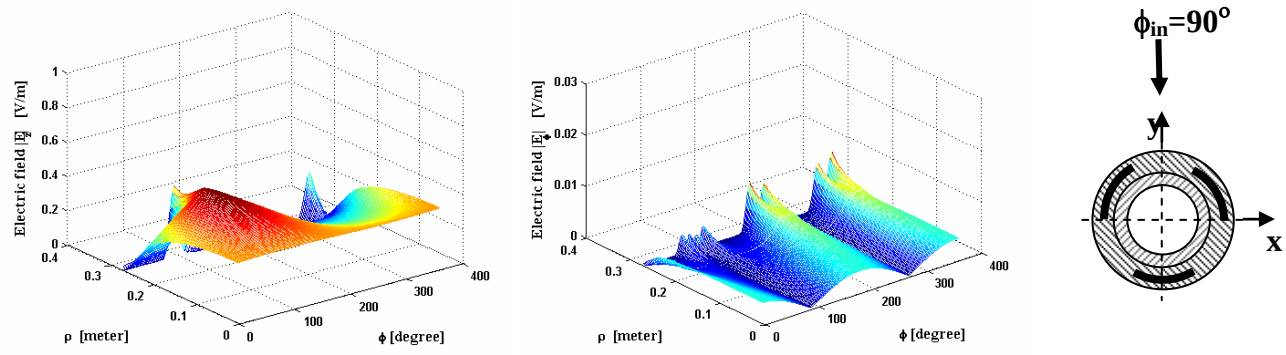

(c) Three patch-array.

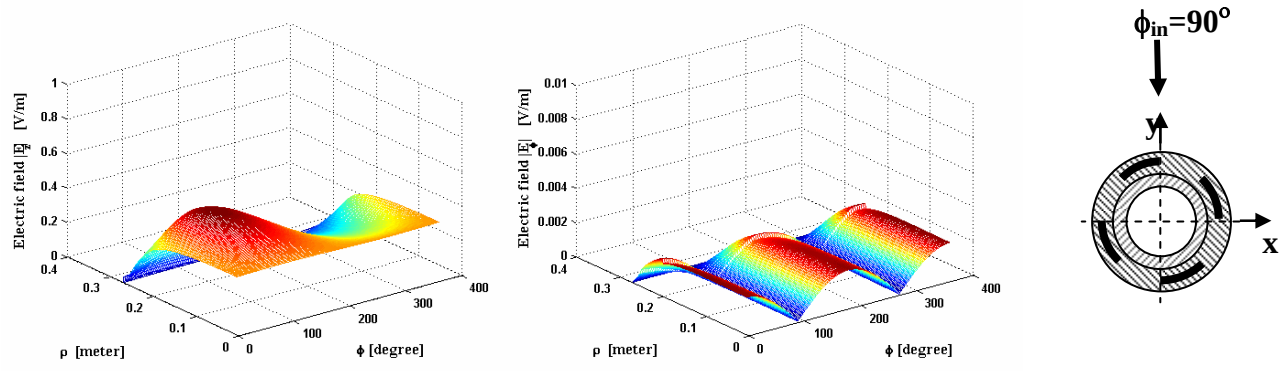

(d) Four patch-array.

Fig. 2 The penetrated fields distributions |Ez| and |Eϕ| for different array geometries.

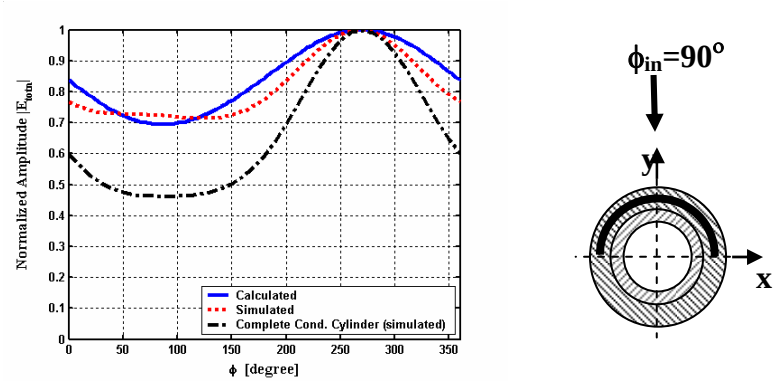

(a) One patch-array.

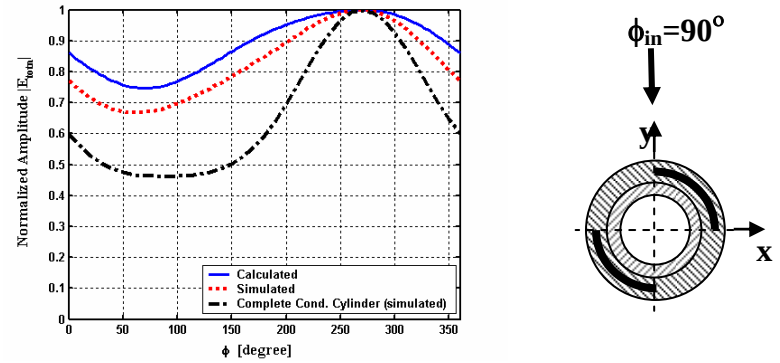

(b) Two patch-array.

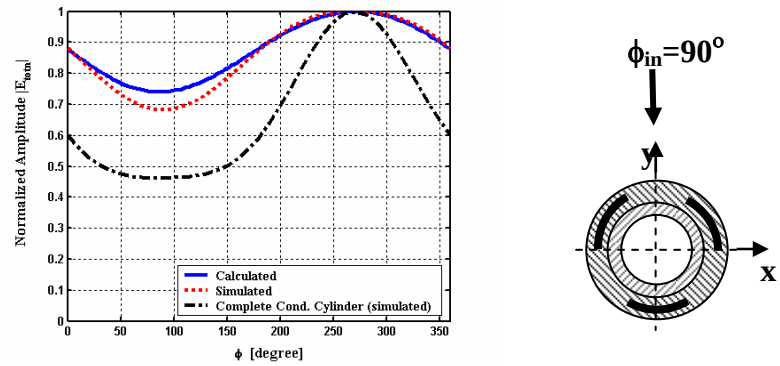

(c) Three patch-array.

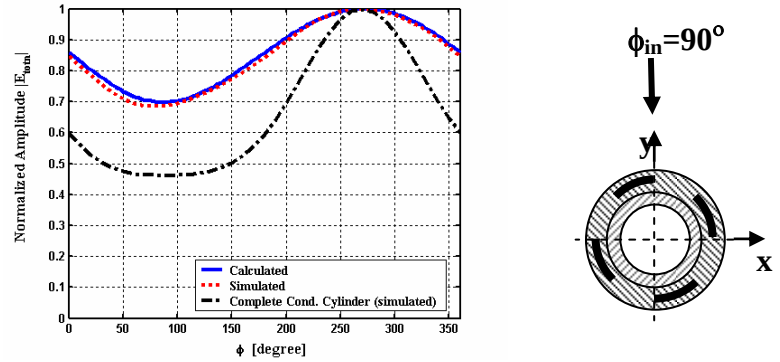

(d) Four patch-array.

Fig. 3 The far zone scattered field for different array geometries.

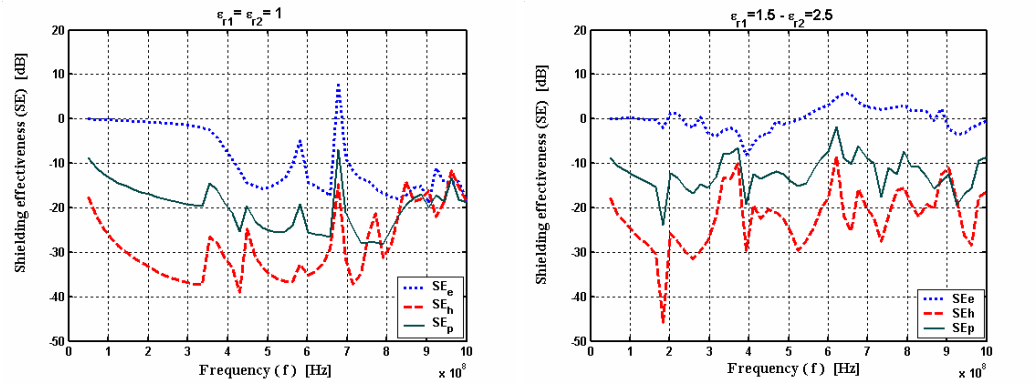

(a) One patch-array.

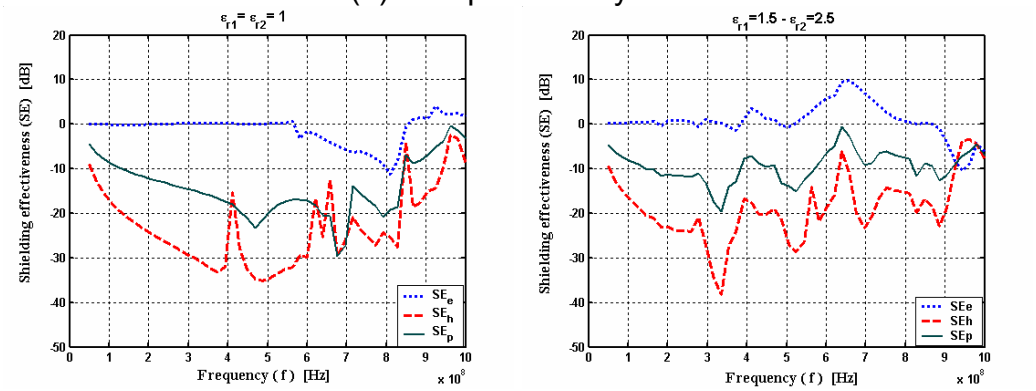

(b) Two patch-array.

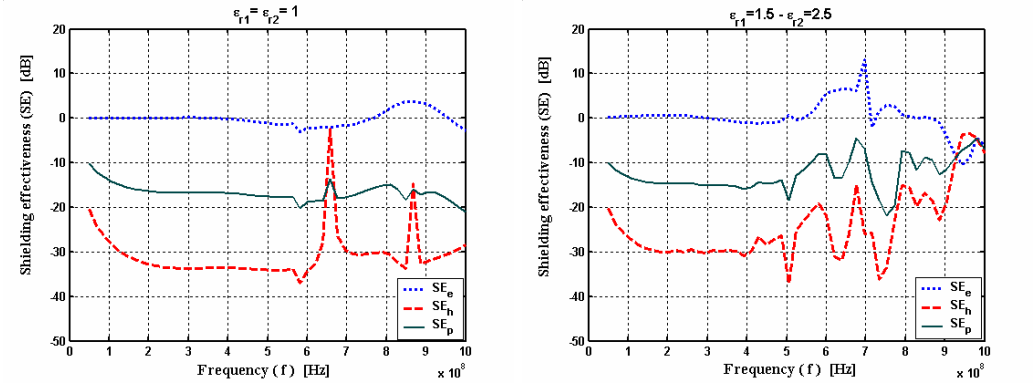

(c) Three patch-array.

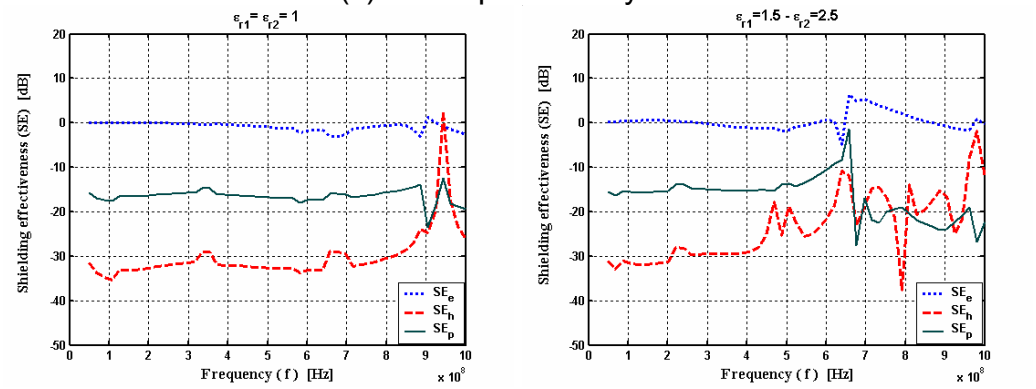

(d) Four patch-array.

Fig. 4 Shielding effectiveness (SE) with and without the presence of dielectric layers for different array geometries at ρ=0.05 m.

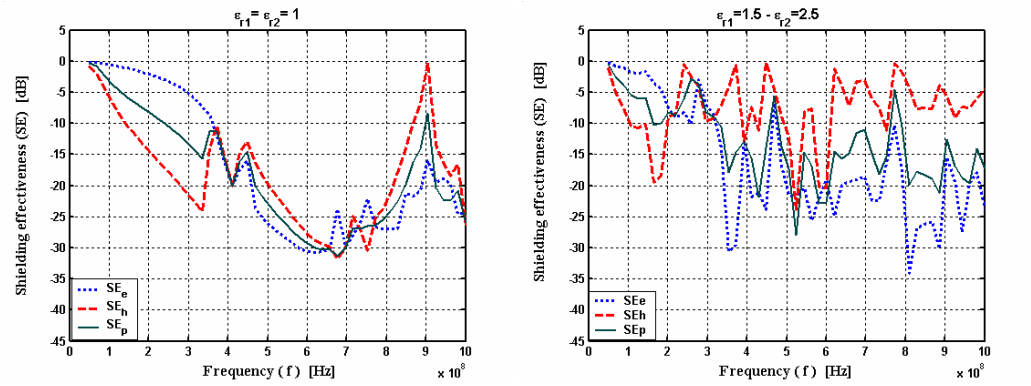

(a) One patch-array.

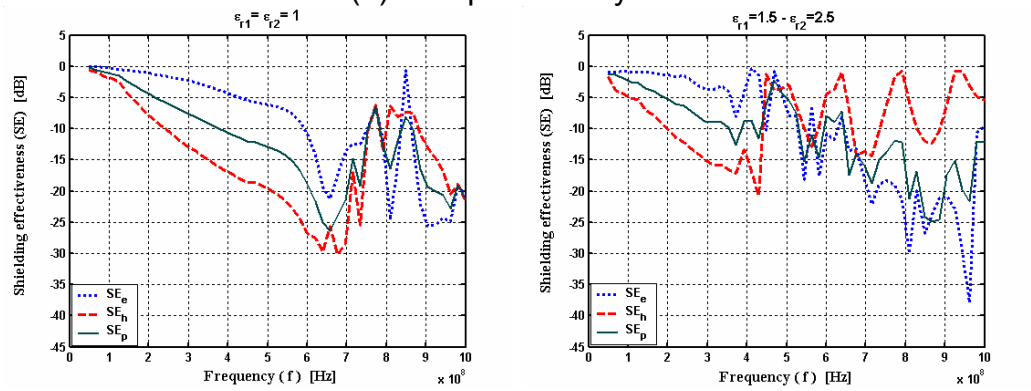

(b) Two patch-array.

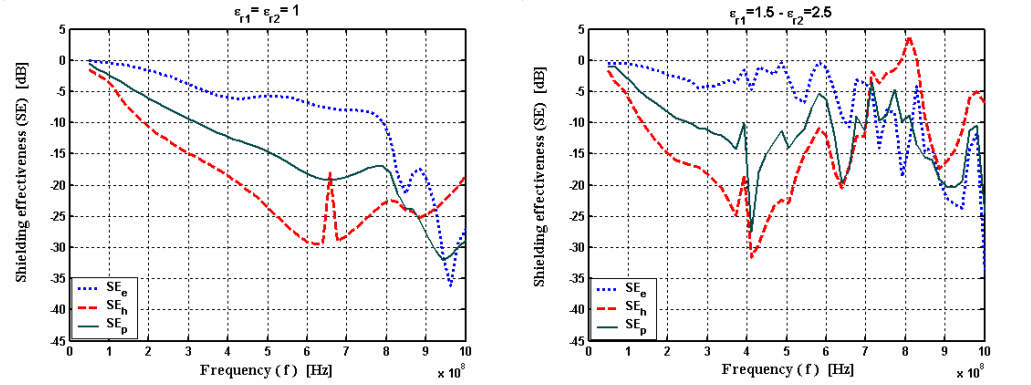

(c) Three patch-array.

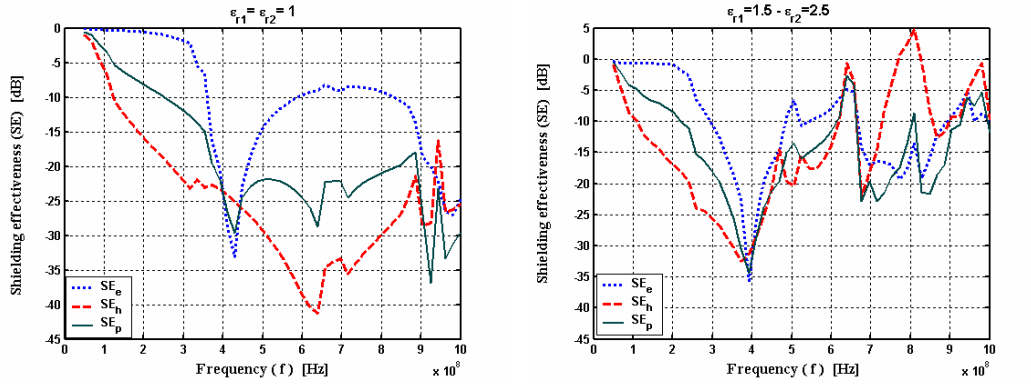

(d) Four patch-array.

Fig. 5 Shielding effectiveness (SE) with and without the presence of dielectric layers for different array geometries at ρ=0.27 m.